



Globally exponentially stable observer for vision-based range estimation

A.P. Dani, N.R. Fischer, Z. Kan, W.E. Dixon*

Department of Mechanical and Aerospace Engineering, University of Florida, Gainesville, FL 32611, United States

ARTICLE INFO

Article history:

Available online 21 November 2011

Keywords:

Structure from motion
Nonlinear observers
Visual servo control
Vision-based localization

ABSTRACT

A reduced-order nonlinear observer is developed to estimate the distance from a moving camera to a feature point on a static object (i.e., range identification), where full velocity and linear acceleration feedback of the calibrated camera is provided. The contribution of this work is to develop a global exponential range observer which can be used for a larger set of camera motions than existing observers. The observer is shown to be robust against external disturbances in the sense that the observer is \mathcal{L}_p -stable even if the target object is moving or the camera motion is perturbed. The presented observer identifies the range provided an observability condition commonly used in literature is satisfied and is shown to be exponentially stable even if camera motion satisfies a less restrictive observability condition. A sufficient condition on the observer gain is derived to prove stability using a Lyapunov-based analysis. Experimental results are provided to show robust performance of the observer using an autonomous underwater vehicle (AUV).

© 2011 Elsevier Ltd. All rights reserved.

1. Introduction

Relative depth information in a scene recovered using a moving camera can be used to estimate the range (and hence, a 3D structure) of tracked feature points in 2D images. The objective of the “structure from motion (SfM)” problem is to estimate the Euclidean geometry (i.e., range or 3D structure) of feature points of interest in a static scene when the motion of the camera is known. The estimated 3D structure information can be used in variety of automatic control and surveillance tasks.

Solutions to the SfM problem can be broadly classified as offline methods (batch methods) and online methods (iterative methods). References and critiques of batch methods can be found in [1–6] and the references therein. Online methods typically formulate the SfM problem as a continuous differential equation, where the image dynamics are derived from a continuous image sequence (see [7–17] and the references therein). Online methods often rely on the use of an Extended Kalman Filter (EKF) [7,18–20]. Stability of the EKF is proven as an observer for deterministic systems but it is well known that the EKF may fail in some real applications [21,22]. For the continuous time EKF, the convergence conditions can only be checked by actually running the filter [23]. The EKF is an approximation method, requires nonlinear dynamics to be linearized, and requires a priori knowledge about the noise covariance. In comparison to Kalman filter-based approaches, some researchers have developed nonlinear observers for SfM with ana-

lytical proofs of stability. For example, a high-gain observer called the identifier-based observer (IBO) is presented for range estimation in the seminal result in [17] under the assumption that camera motion is known. In [12], a discontinuous sliding-mode observer is developed which guarantees exponential convergence of the states to an arbitrarily small neighborhood, i.e., the state estimation error is uniformly ultimately bounded (UUB) to a small ball around the origin of the system. A semi-globally asymptotically stable reduced-order observer is presented in [24] to estimate the range of a stationary object using a known camera motion. A continuous observer which guarantees asymptotic range estimation is presented in [13] under the assumption that camera motion is known. In [15], an asymptotically converging nonlinear observer is developed based on Lyapunov’s indirect method. An application of the IBO is presented in [25] to estimate the range of features in a static scene.

Recently in [26], a nonlinear observer was developed that identifies the distance to a target exponentially fast provided a persistency of excitation (PE) condition is satisfied. The observer requires the initial condition be close to the ‘true’ depth (i.e., a local result). It is noted that the observer is guaranteed to converge with initial conditions in an arbitrarily large compact set if the linear velocity in the forward direction, and two angular velocities are small. The authors in [26] propose that the camera velocities can be kept small by using a visual servoing controller scheme and restricting the domain of applications for the observer. In another recent work [27], an immersion and invariance (I&I) based approach is used to design a reduced-order observer to achieve global exponential convergence of the estimation error. The observer requires camera

* Corresponding author. Tel.: +1 352 846 1463; fax: +1 352 391 7303.

E-mail address: wdixon@ufl.edu (W.E. Dixon).

velocity and acceleration measurements along with feature point measurements from the image. The authors state that the observer has to satisfy the Extended Output Jacobian (EOJ) observability rank condition, which is more strict than the PE condition. Thus, the observer in [27] cannot address all of the camera motions achieved by the observer in [26]. The gain condition of the observer in [27] is a function of image features, camera velocities and camera accelerations.

In this paper, globally exponentially stable reduced-order observer is developed with a less restrictive observability condition than in other results. The derived gain condition is only a function of the upper bounds on camera velocities and image size. The result is achieved provided an observability condition is met, which is the same physically motivated condition required by most observers available in literature (cf. [12,13,24,25]). If the observability condition is violated, the proposed observer can still be applied as a local observer, similar to [26]. The observation error is shown to be finite-gain $\mathcal{L}_p \forall p \in [1, \infty]$ stable with respect to an exogenous disturbance acting on the system. The observer errors remain within a bound which can be reduced by tuning the observer gains. Results using both synthetic data and experimental data are provided to show the performance of the developed observer. Multiple camera trajectories are also analyzed to illustrate the performance of the observer in different observability conditions. Simulations compare the current result with the results in [26,27]. This comparison highlights the advantages of the global nature of the result and the fact that the observer does not include a singularity.

2. Mapping from Euclidean to image space

A moving camera observing a static scene induces feature motion in the image plane. Point correspondences between consecutive images can be computed using existing feature tracking techniques [28–30].

Let \mathcal{F}^* be an orthogonal coordinate system attached to the camera at the location corresponding to an initial point in time, t_0 . After the initial time, let an orthogonal coordinate system attached to the camera which has undergone some rotation $\bar{R}(t) \in SO(3)$ and translation $\bar{x}_f(t) \in \mathbb{R}^3$ away from \mathcal{F}^* be denoted as \mathcal{F}_c . Let $\bar{m}(t) \in \mathbb{R}^3$ denote the Euclidean coordinates of a feature point observed by the moving camera expressed in the camera frame \mathcal{F}_c and $m(t) \in \mathbb{R}^3$ denote the respective normalized Euclidean coordinates, defined as

$$\bar{m}(t) = [x_1(t), x_2(t), x_3(t)]^T, \tag{1}$$

$$m(t) = \begin{bmatrix} x_1(t) & x_2(t) \\ x_3(t) & x_3(t) \end{bmatrix}^T. \tag{2}$$

Consider a closed and bounded set $\mathcal{Y} \subset \mathbb{R}^3$. To facilitate the subsequent development, an auxiliary state vector $y(t) = [y_1(t), y_2(t), y_3(t)]^T \in \mathcal{Y}$ is constructed from (2) as

$$y = \begin{bmatrix} x_1 & x_2 & 1 \\ x_3 & x_3 & x_3 \end{bmatrix}^T. \tag{3}$$

Using projective geometry, the normalized Euclidean coordinates $m(t)$ can be related to the pixel coordinates in the image space as

$$p = Am, \tag{4}$$

where $p(t) = [u \ v \ 1]^T$ is a vector of the image-space feature point coordinates $u(t)$, $v(t) \in \mathbb{R}$ defined on the closed and bounded set $\mathcal{I} \subset \mathbb{R}^3$, and $A \in \mathbb{R}^{3 \times 3}$ is a constant, known, invertible intrinsic camera calibration matrix [31]. The expression in (4) can be used to recover $m(t)$, which can be used to partially reconstruct the state $y(t)$ so that the first two components of $y(t)$ can be determined.

Assumption 1. The camera velocities are assumed to be bounded, and the linear velocities are assumed to be continuously differentiable.

Remark 1. The states $y_1(t)$ and $y_2(t)$ represent pixel locations. From the finite size of the image, $y_1(t)$ and $y_2(t)$ are bounded by known constants as

$$\underline{y}_1 \leq y_1(t) \leq \bar{y}_1, \quad \underline{y}_2 \leq y_2(t) \leq \bar{y}_2.$$

The relative Euclidean distance $x_3(t)$ between the camera and the feature point is lower bounded by the camera focal length λ_m (in meters), and is not assumed to be upper bounded. Therefore, the state $y_3(t)$, an inverse of the state $x_3(t)$, can be upper and lower bounded as [26]

$$0 < \underline{y}_3 < y_3(t) \leq \frac{1}{\lambda_m} = \bar{y}_3.$$

3. Perspective camera motion model

As seen from Fig. 1, the static scene point q can be expressed in the coordinate system \mathcal{F}_c as

$$\bar{m} = \bar{x}_f + \bar{R}x_{Oq}, \tag{5}$$

where x_{Oq} is a vector from the origin of coordinate system \mathcal{F}^* to the static point q expressed in the coordinate system \mathcal{F}^* . Differentiating (5), the relative motion of q as observed in the camera coordinate system can be expressed by the following kinematics [31,32]

$$\dot{\bar{m}} = [\omega]_{\times} \bar{m} + b, \tag{6}$$

where $\bar{m}(t)$ is defined in (1), $[\omega]_{\times} \in \mathbb{R}^{3 \times 3}$ denotes a skew symmetric matrix formed from the angular velocity vector of the camera $\omega(t) = [\omega_1 \ \omega_2 \ \omega_3]^T \in \mathcal{W}$, and $b(t) = [b_1 \ b_2 \ b_3]^T \in \mathcal{B}$ denotes the linear velocity of the camera. The sets \mathcal{W} and \mathcal{B} are closed and bounded sets such that $\mathcal{W} \subset \mathbb{R}^3$ and $\mathcal{B} \subset \mathbb{R}^3$. By re-arranging the expression in (6), the motion of a stationary point as observed by a moving camera can also be expressed as

$$\dot{\bar{m}} = \begin{bmatrix} 1 & 0 & 0 & 0 & x_3 & -x_2 \\ 0 & 1 & 0 & -x_3 & 0 & x_1 \\ 0 & 0 & 1 & x_2 & -x_1 & 0 \end{bmatrix} \begin{bmatrix} b \\ \omega \end{bmatrix}. \tag{7}$$

Using (3) and (7), the dynamics of the partially measurable state $y(t)$ can be expressed as

$$\begin{aligned} \dot{y}_1 &= (b_1 - y_1 b_3) y_3 - y_1 y_2 \omega_1 + (1 + y_1^2) \omega_2 - y_2 \omega_3, \\ \dot{y}_2 &= (b_2 - y_2 b_3) y_3 - (1 + y_2^2) \omega_1 + y_1 y_2 \omega_2 + y_1 \omega_3, \\ \dot{y}_3 &= -y_3^2 b_3 - y_2 y_3 \omega_1 + y_1 y_3 \omega_2, \end{aligned} \tag{8}$$

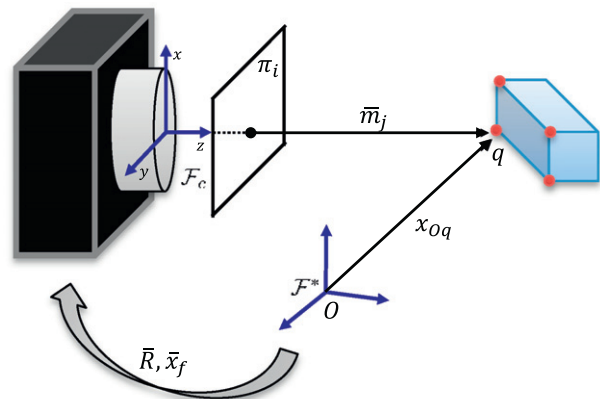


Fig. 1. Moving camera looking at the static scene.

where the states $y_1(t)$ and $y_2(t)$ can be measured as the output of the system through the invertible transformation given by (4). The following symbols are defined to streamline the notations throughout the paper:

$$h_1 \triangleq b_1 - y_1 b_3, \quad h_2 \triangleq b_2 - y_2 b_3, \quad p_1 \triangleq -y_1 y_2 \omega_1 + (1 + y_1^2) \omega_2 - y_2 \omega_3 \text{ and } p_2 \triangleq -(1 + y_2^2) \omega_1 + y_1 y_2 \omega_2 + y_1 \omega_3.$$

4. Vision-based range estimation

The objective of the range estimation problem (i.e., SfM) is to estimate the Euclidean coordinates of feature points in a static scene using a moving camera with known camera velocities $b(t)$ and $\omega(t)$. The projective transformation onto the image plane loses depth information, but it can be recovered from 2D point correspondences in the images. Once the Euclidean depth is recovered using (3) and (4), the complete Euclidean coordinates can be computed.

4.1. Range observer

In this section, a new nonlinear observer for range estimation is presented. The dynamics of the range, given by $\bar{m}(t)$, are represented using the perspective dynamic system in (8). All six velocities and linear accelerations of the camera are available as *sensor measurements*. Scenarios where the relative motion $\omega(t)$ and $b(t)$ are known include a camera attached to the end-effector of a robot manipulator, mobile robot, autonomous underwater vehicle (AUV), or micro air vehicle (MAV). Linear and angular camera velocity, and linear camera acceleration can be acquired using a wide array of sensor configurations utilizing an inertial measurement unit (IMU), global positioning system (GPS), or other sensors.

The state $y_3(t)$ contains depth information which is lost due to a perspective transformation. To obtain the range of a feature point $\bar{m}(t)$, it is necessary to scale the measured states $y_1(t)$ and $y_2(t)$ using the depth. Thus, the main motivation of the observer is to estimate the state $y_3(t)$. Let the estimates of the state $y_3(t)$ be defined as $\hat{y}_3(t)$. To quantify the depth estimation mismatch, an estimate error $e(t)$ is defined as

$$e \triangleq y_3 - \hat{y}_3. \tag{9}$$

To ensure the estimate $\hat{y}_3(t)$ is bounded, a locally Lipschitz projection law [33] is designed to update $\hat{y}_3(t)$ as

$$\dot{\hat{y}}_3(t) = \text{proj}(\dot{y}_3, \phi) = \begin{cases} \phi & \begin{cases} \text{if } \underline{y}_3 \leq \hat{y}_3(t) \leq \bar{y}_3 \text{ or} \\ \hat{y}_3(t) > \bar{y}_3 \text{ and } \phi(t) \leq 0 \text{ or} \\ \hat{y}_3(t) < \underline{y}_3 \text{ and } \phi(t) \geq 0 \end{cases} \\ \bar{\phi} & \text{if } \hat{y}_3(t) > \bar{y}_3 \text{ and } \phi(t) > 0 \\ \check{\phi} & \text{if } \hat{y}_3(t) < \underline{y}_3 \text{ and } \phi(t) < 0 \end{cases}, \tag{10}$$

where $\phi(y_1, y_2, \hat{y}_3, b_3, e_1, e_2) \in \mathbb{R}$ is defined as

$$\phi \triangleq \hat{y}_3^2 b_3 + (y_2 \omega_1 - y_1 \omega_2) \hat{y}_3 - k_3 (h_1^2 + h_2^2) \hat{y}_3 + k_3 (-h_1 p_1 - h_2 p_2 + h_1 \dot{y}_1 + h_2 \dot{y}_2), \tag{11}$$

and $\bar{\phi}(t) \in \mathbb{R}$ and $\check{\phi}(t) \in \mathbb{R}$ are defined as

$$\bar{\phi} \triangleq \left[1 + \frac{\bar{y}_3 - \hat{y}_3}{\delta} \right] \phi, \quad \check{\phi} \triangleq \left[1 + \frac{\hat{y}_3 - \underline{y}_3}{\delta} \right] \phi. \tag{12}$$

The projection in (10) ensures that the estimate $\hat{y}_3 \in \Omega_\delta \forall t \geq 0$, where $\Omega_\delta = \{\hat{y}_3 \mid \underline{y}_3 - \delta \leq \hat{y}_3 \leq \bar{y}_3 + \delta\}$ for some known arbitrary constant $\delta > 0$. The signal $\phi(t)$ can be integrated to eliminate the

computation of optical flow, i.e., \dot{y}_1 and \dot{y}_2 , and the signal \hat{y}_3 can be generated using

$$\dot{\hat{y}}_3 = \alpha + \beta. \tag{13}$$

Instead of (11), in (13) the update law for the function $\alpha(y_1, y_2, \hat{y}_3, \omega, b, \dot{b})$ is given by

$$\begin{aligned} \alpha = & \hat{y}_3^2 b_3 + (y_2 \omega_1 - y_1 \omega_2) \hat{y}_3 - k_3 (h_1^2 + h_2^2) \hat{y}_3 - k_3 h_1 p_1 \\ & - k_3 h_2 p_2 - k_3 y_1 \dot{b}_1 - k_3 y_2 \dot{b}_2 + k_3 \dot{b}_3 \left(\frac{y_1^2 + y_2^2}{2} \right) \end{aligned} \tag{14}$$

and $\beta(y_1, y_2, b)$ is defined as

$$\beta \triangleq k_3 \left(b_1 y_1 + b_2 y_2 - b_3 \left(\frac{y_1^2 + y_2^2}{2} \right) \right), \tag{15}$$

where $k_3 \in \mathbb{R}^+$. The initial condition of the observer is selected as

$$\alpha(t_0) = \alpha_0$$

where α_0 is an arbitrary constant.

Assumption 2. The subsequent development is based on the assumption that $h_1^2 + h_2^2 \geq \varepsilon > 0, \forall t \geq 0$ for a positive constant ε . This assumption is an observability condition for the observer in (10)–(15), and is the same as obtained previously in the literature [13,17,27,34]. The condition physically implies that $b_1(t), b_2(t), b_3(t)$ are not equal to zero simultaneously and the motion of the camera should not be along the projected ray of the point being observed.

Theorem 1. *The observer presented in (10)–(15) is a globally exponentially stable observer provided Assumption 1 is satisfied along with the sufficient condition*

$$k_3 \geq \frac{2\bar{b}_3 + \delta\bar{b}_3 + \bar{y}_2\bar{\omega}_1 + \bar{y}_1\bar{\omega}_2}{\varepsilon} \tag{16}$$

where $\bar{b}_3, \bar{\omega}_1$ and $\bar{\omega}_2$ are known upper bounds on $b_3(t), \omega_1(t)$ and $\omega_2(t)$.

Proof. For three cases of projection law described by (10) the $e(t)$ error dynamics are given by

Case 1: $\underline{y}_3 \leq \hat{y}_3(t) \leq \bar{y}_3$ or $\hat{y}_3(t) > \bar{y}_3$ and $\phi(t) \leq 0$ or $\hat{y}_3(t) < \underline{y}_3$ and $\phi(t) \geq 0$. Using (8) and (10)–(12), the error dynamics of $e(t)$ can be expressed as

$$\dot{e} = \zeta \triangleq (y_2 \omega_1 - y_1 \omega_2) e + (y_3 + \hat{y}_3) b_3 e - k_3 (h_1^2 + h_2^2) e. \tag{17}$$

Case 2: $\hat{y}_3(t) > \bar{y}_3$ and $\phi(t) > 0$. Using (8) and (10)–(12), the error dynamics of $e(t)$ can be expressed as

$$\dot{e} = \zeta - \frac{\bar{y}_3 - \hat{y}_3}{\delta} \phi. \tag{18}$$

Case 3: $\hat{y}_3(t) < \underline{y}_3$ and $\phi(t) < 0$. Using (8) and (10)–(12), the error dynamics of $e(t)$ can be expressed as

$$\dot{e} = \zeta - \frac{\hat{y}_3 - \underline{y}_3}{\delta} \phi. \tag{19}$$

The stability of the proposed observer can be analyzed using Lyapunov-based stability analysis. Consider a domain $\mathcal{D} \subset \mathbb{R}$ containing $e(0)$ and a continuously differentiable, radially unbounded candidate Lyapunov function, $V(e) : \mathcal{D} \times [0, \infty) \rightarrow \mathbb{R}^+$, defined as

$$V \triangleq \frac{1}{2} e^2. \tag{20}$$

The stability of the error system will be analyzed for all three cases of the projection law.

Case 1: Taking the derivative of $V(e)$ and utilizing (17) yields

$$\dot{V} = \left[(y_3 + \hat{y}_3)b_3 - y_2\omega_1 + y_1\omega_2 - k_3(h_1^2 + h_2^2) \right] e^2. \quad (21)$$

If k_3 satisfies the condition in (16), the bracketed term is strictly negative and the following expression is obtained

$$\dot{V} \leq -k_1 V, \quad (22)$$

where $k_1 \in \mathbb{R}^+$.

Case 2: Taking the derivative of $V(e)$ and utilizing (18) yields

$$\begin{aligned} \dot{V} = & ((y_3 + \hat{y}_3)b_3 - y_2\omega_1 + y_1\omega_2)e^2 - k_3(h_1^2 + h_2^2)e^2 \\ & - e \frac{\bar{y}_3 - \hat{y}_3}{\delta} \phi, \end{aligned} \quad (23)$$

where the last term on the right hand side of (23) is always negative, and hence, the inequality in (22) can be achieved.

Case 3: Taking the derivative of $V(e)$ and utilizing (19) yields

$$\begin{aligned} \dot{V} = & ((y_3 + \hat{y}_3)b_3 - y_2\omega_1 + y_1\omega_2)e^2 - k_3(h_1^2 + h_2^2)e^2 \\ & - e \frac{\hat{y}_3 - y_3}{\delta} \phi, \end{aligned} \quad (24)$$

where the last term on the right hand side of (24) is always negative, and hence, the inequality in (22) can be achieved.

For all three cases of projection the Gronwall-Bellman lemma [35] can be applied to (22) to yield

$$V(t) \leq V(0) \exp(-k_1 t).$$

Hence, from (20), the following upper bound for $e(t)$ can be obtained

$$\|e(t)\| \leq \gamma \|e(0)\| \exp(-k_1 t), \quad (25)$$

where $\gamma \in \mathbb{R}^+$.

From (25), $e(t) \in \mathcal{L}_\infty$.¹ Since $e(t) \in \mathcal{L}_\infty$, and using Remark 1, $y_3(t) \in \mathcal{L}_\infty$, thus $\hat{y}_3(t) \in \mathcal{L}_\infty$. From the boundedness of $y(t)$, $b(t)$ and $\omega(t)$, and Assumption 2, (16) can be used to prove that $k_3 \in \mathcal{L}_\infty$. Based on the fact that $e(t)$, $y(t)$, $\omega(t)$, $b(t)$, $k_3 \in \mathcal{L}_\infty$, standard linear analysis methods can be used to prove that $\dot{e}(t) \in \mathcal{L}_\infty$. Thus, $y_3(t)$ is exponentially estimated and (2)–(4) can be used to recover the Euclidean coordinates $\bar{m}(t)$ of the feature point. \square

If the condition in Assumption 2 is not satisfied and the gain k_3 is chosen according to (16), the proposed observer is still exponentially convergent, provided the PE condition in [26] is satisfied.

Theorem 2. *The observer presented in (10)–(15) is a exponentially stable observer provided k_3 is chosen according to (16), Assumption 1 is satisfied, and the following PE condition is satisfied*

$$\int_t^{t+T} (h_1^2(\tau) + h_2^2(\tau)) d\tau \geq \rho > 0, \quad \forall t > 0, \quad (26)$$

where $T, \rho \in \mathbb{R}^+$.

Proof. To examine the stability of the estimation error dynamics in (17) under the assumption that (26) is satisfied, consider the nominal system

$$\dot{e} = -k_3(h_1^2 + h_2^2)e. \quad (27)$$

Using Theorem 2.5.1 of [36] the error system in (27) is globally exponentially stable if the condition in (26) is satisfied. Since the nominal system in (27) is globally exponentially stable using Theorem 4.14 of [37], based on the Converse Lyapunov Theorem there exists a function $\bar{V} : [0, \infty) \times \mathbb{R} \rightarrow \mathbb{R}$ that satisfies the inequalities

$$\begin{aligned} c_1 \|e\|^2 &\leq \bar{V}(t, e) \leq c_2 \|e\|^2, \\ \frac{\partial \bar{V}}{\partial t} + \frac{\partial \bar{V}}{\partial e} (-k_3(h_1^2 + h_2^2)e) &\leq -c_3 \|e\|^2, \\ \left\| \frac{\partial \bar{V}}{\partial e} \right\| &\leq c_4 \|e\| \end{aligned} \quad (28)$$

where $c_i \in \mathbb{R}^+$, $\forall i = \{1, \dots, 4\}$. After using (20) with the properties in (28) and substituting in the perturbed system (17), the following inequalities can be obtained

$$\begin{aligned} \dot{\bar{V}} &\leq \frac{\partial \bar{V}}{\partial t} + \frac{\partial \bar{V}}{\partial e} (-k_3(h_1^2 + h_2^2)e), \\ &\quad + \frac{\partial \bar{V}}{\partial e} ((y_3 + \hat{y}_3)b_3 - y_2\omega_1 + y_1\omega_2)e, \end{aligned}$$

$$\dot{\bar{V}} \leq -c_3 \|e\|^2 + c_4 \eta \|e\|^2,$$

where $\eta = \frac{2b_3}{\lambda} + \delta \bar{b}_3 + \bar{y}_2 \bar{\omega}_1 + \bar{y}_1 \bar{\omega}_2$, and $\dot{\bar{V}}(t)$ can be upper bounded as

$$\dot{\bar{V}} \leq -(c_3 - \eta c_4) \|e\|^2.$$

Since k_3 is selected according to (16) with sufficiently small δ , c_3 satisfies $c_3 > \eta c_4$. Hence, the origin of the perturbed system (17) is exponentially stable. \square

Remark 2. As stated in [26], the PE condition physically implies that all the linear velocities should not be identically zero and that the camera should not be translating along the projected ray of any feature point during any small interval of time $[t, t + T]$. If all of the linear velocities are zero at any instant of time $h_1^2(t) + h_2^2(t) = 0$ and the stability of the observer in (10)–(15) cannot be shown using Theorem 1, Theorem 2 ensures stability of system in such cases.

5. Stability analysis in the presence of disturbances

In this section, the stability of the observer in (10)–(15) is analyzed in the presence of an exogenous input such as a disturbance acting on the camera motion or a target object begins to move. The disturbance enters the system as

$$\dot{\bar{m}} = \begin{bmatrix} 1 & 0 & 0 & 0 & -x_3 & x_2 \\ 0 & 1 & 0 & x_3 & 0 & -x_1 \\ 0 & 0 & 1 & -x_2 & x_1 & 0 \end{bmatrix} \begin{bmatrix} b + \Delta b \\ \omega + \Delta \omega \end{bmatrix}, \quad (29)$$

where $\Delta b(t)$, $\Delta \omega(t)$ represent the exogenous inputs such that $\Delta b(t)$, $\Delta \omega(t) \in \mathcal{L}_{pe}$ ² with $\sup_{0 \leq t \leq \tau} \|\Delta b(t)\| \leq r_b$ and $\sup_{0 \leq t \leq \tau} \|\Delta \omega(t)\| \leq r_\omega$ for some $r_b, r_\omega \in \mathbb{R}^+$. Using (3) and (29), the dynamics of the unmeasurable state $y_3(t)$ can be expressed as

$$\dot{y}_3 = -y_3^2 b_3 - y_2 y_3 \omega_1 + y_1 y_3 \omega_2 + \Delta y_3, \quad (30)$$

where

$$\Delta y_3 = -y_3^2 \Delta b_3 - y_2 y_3 \Delta \omega_1 + y_1 y_3 \Delta \omega_2.$$

¹ For a function $s(t) \in \mathbb{R}^n \forall n \in [1, \infty)$, $s(t) \in \mathcal{L}_\infty$ means the function $s(t)$ has a finite \mathcal{L}_∞ norm, i.e., $\|s(t)\|_{\mathcal{L}_\infty} = \sup_{t \geq 0} \|s(t)\|_2 < \infty$ where $\|\cdot\|_2$ denotes the 2-norm in \mathbb{R}^n .

² The space $\mathcal{L}_{pe} = \{u|u_\tau \in \mathcal{L}_p, \forall \tau \in [0, \infty)\}$, and u_τ is a truncation of u defined by $u_\tau(t) = \begin{cases} u(t), & 0 \leq t \leq \tau \\ 0, & t > \tau \end{cases}$.

Table 1
Comparison of the presented observer with observers in [26,27].

Observer in this paper	Observer via I&I [27]	Observer in [26]
Global exponential error convergence Observability: $h_1^2(t) + h_2^2(t) \geq \varepsilon > 0, \forall t \geq 0$, stable if $\exists t : h_1^2(t) + h_2^2(t) = 0$ Requires camera velocities and linear accelerations Reduced order	Global exponential error convergence Observability: $h_1^2(t) + h_2^2(t) \geq \varepsilon > 0, \forall t \geq 0$ singular if $h_1^2(t) + h_2^2(t) = 0$ for any time t Requires camera velocities and linear accelerations Reduced order	Local exponential error convergence Observability: $\exists \bar{t} : \forall t > \bar{t}, h_1^2(t) + h_2^2(t) = 0$ stable if $\exists t : h_1^2(t) + h_2^2(t) = 0$ Requires only camera velocities Full order

Theorem 3. The observer presented in (10)–(15) is finite-gain \mathcal{L}_p^3 stable where $p \in [1, \infty]$ with respect to the exogenous input $[\Delta b^T \Delta \omega^T]^T$ and \mathcal{L}_p gain less than or equal to $\frac{1}{k_1}$.

Proof. Using (30) and (10)–(15) the error system can be written as

$$\dot{e} = (y_2\omega_1 - y_1\omega_2)e + (y_3 + \dot{y}_3)b_3e - k_3(h_1^2 + h_2^2)e + \Delta y_3k_3. \quad (31)$$

The error system in (31) can be expressed in the following form

$$\begin{aligned} \dot{e} &= f(e, u), \\ r &= h(e), \end{aligned}$$

where $u(t) = k_3\Delta y_3(t)$ is an exogenous disturbance/noise input, $r(t) = e(t)$. Let \mathbb{R} be a domain containing $e(t) = 0$ and $u(t) = 0$, the function $f : \mathbb{R} \times \mathbb{R} \rightarrow \mathbb{R}$ is linear and globally Lipschitz in $u(t)$, $h : \mathbb{R} \rightarrow \mathbb{R}$ is continuous in $e(t)$. Using Theorem 1, the unforced system

$$\dot{e} = f(e, 0)$$

is globally exponentially stable with the Lyapunov function in (20) which satisfies the following bounds

$$\begin{aligned} 0.5\|e\|^2 &\leq V(e) \leq 0.5\|e\|^2, \\ \frac{\partial V}{\partial t} + \frac{\partial V}{\partial e}(f(e, 0)) &\leq -k_1\|e\|^2, \\ \left\| \frac{\partial V}{\partial e} \right\| &\leq \|e\|. \end{aligned} \quad (32)$$

Since the function $f(e, u)$ is globally Lipschitz in $u(t)$, the following inequality is satisfied

$$\|f(e, u) - f(e, 0)\| \leq \|u\|. \quad (33)$$

Since (32) and (33) are satisfied, using Theorem 5.1 of [37] the error system in (31) is finite gain \mathcal{L}_p stable where $p \in [1, \infty]$ with \mathcal{L}_p gain less than or equal to $\frac{1}{k_1}$ for each $e(0) \in \mathbb{R}$, i.e.,

$$\|e\|_{\mathcal{L}_p} \leq \frac{1}{k_1} \|u\|_{\mathcal{L}_p} + \|e_0\|_{\rho},$$

where

$$\rho = \begin{cases} 1, & \text{if } n = \infty \\ \left(\frac{1}{k_1^n}\right)^{1/n}, & \text{if } n \in [1, \infty) \end{cases}$$

The velocities of the object denoted by b_0 and ω_0 can be assumed to be \mathcal{L}_{pe} disturbances acting on the system as shown in (29). Thus, Theorem 3 implies that even if the stationary object assumption is violated, the observer errors are bounded. The \mathcal{L}_p gain is the measure of accuracy of the estimates and gives an upper bound on the estimation errors. The \mathcal{L}_p gain can be reduced by increasing the gain k_3 which in turn reduces the constant k_1 (see (21) and (22)). \square

³ A mapping $F : \mathcal{L}_e^m \rightarrow \mathcal{L}_e^n$ is finite-gain \mathcal{L} stable if there exist non-negative constants ϱ and χ such that $\|(Fu)\|_{\mathcal{L}} \leq \varrho\|u\|_{\mathcal{L}} + \chi$ for all $u \in \mathcal{L}_e^m$ and $\tau \in [0, \infty)$ where the extended space \mathcal{L}_e^m is defined as $\mathcal{L}_e^m = \{u|u_{\tau} \in \mathcal{L}^m, \forall \tau \in [0, \infty)\}$.

6. Discussion

A comparison between the observer presented in this paper with the I&I observer [27] and the observer in [26] is provided in Table 1 and the numbered list below.

1. The presented observer achieves *global* exponential estimation of the 3D Euclidean coordinates of feature points, which is a similar result achieved by the observer developed in [27]. The observer presented in [26] only achieves *local* exponential convergence of the estimation errors. Thus, the observers presented in this paper and in [27] can have arbitrary initial conditions as opposed to the initial conditions required by the observer presented in [26]. A limitation of the local nature of the result in [26] is illustrated in the subsequent simulations.
2. One of the advantages of the observer presented in [26] over the observer in [27], is the use of a less restrictive observability condition which enables the observer to be used for a larger set of camera motions. The observability condition in this paper is the same as that in [27], but if the observability condition in [27] is not satisfied, the I&I observer becomes singular. The advantage of the observer in this paper is that even if the observability condition in Assumption 2 is not satisfied, the observer is still locally exponentially stable and thus can encompass a larger set of camera motions. The limitations of the singularity issue with the observer in [27] is illustrated in Section 7.
3. The proposed observer requires measurements of the camera linear acceleration along with camera velocities and image features, which are also required by the observer in [27]. Thus, the observers presented in this paper and in [27] are more sensitive to noisy input measurements compared to the observer in [26]. Improved steady-state performance is illustrated by the observer in [26] in the presence of noise in Section 7.
4. The gain condition in [27] is a function of the image size, camera velocities and acceleration. On the contrary, the gain condition for the observer in this paper is only a function of image size and camera velocities.

7. Simulations and experiments

Simulations are conducted to evaluate the performance of the observer. The performance of the observer is compared with the observers in [26,27]. For each simulation the focal length of the camera is set to $\lambda = 30$ and the gains for the estimators are adjusted to achieve the best performance (i.e., the least estimation error). In contrast to the trial-and-error approach, methodological approaches such as [38–40] could be used to adjust the observer gains. For the first simulation, the initial location of the point on the target with respect to the initial camera frame is selected as $\bar{m}(t_0) = [10 \ 5 \ 0.5]^T$ m. The camera velocities are selected as

$$b = \left[0.3 \ 0.4 + 0.1 \sin\left(\frac{\pi t}{4}\right) \ -0.3 \right]^T \text{ m/s,}$$

$$\omega = \left[0 \ -\frac{\pi}{30} \ 0 \right]^T \text{ rad/s.}$$

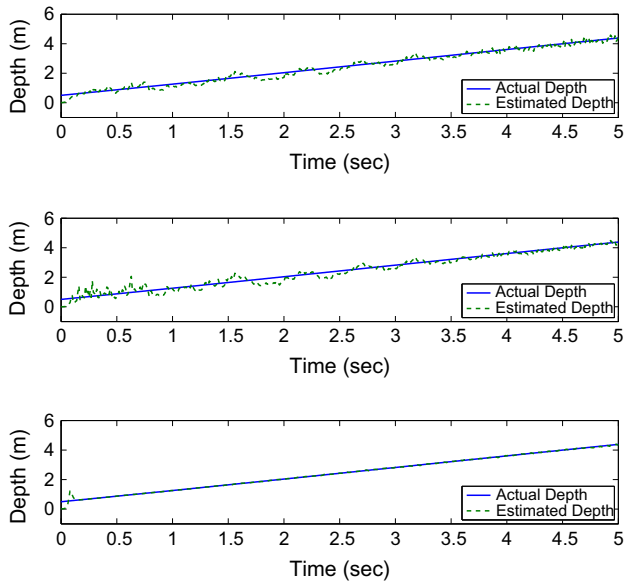


Fig. 2. Comparison between the true and estimated depth in the presence of measurement noise, (a) the top subplot shows the estimated depth using the observer presented in this paper, (b) the middle subplot shows the estimated depth using the observer in [27], (c) the bottom subplot shows the estimated depth using the observer in [26].

Table 2
Comparison of the RMS depth estimation errors.

	Observer in this paper	Observer in [26]	Observer in [27]
Transient RMS error	0.3128	0.3477	0.3547
Steady-state RMS error	0.1717	0.0155	0.2150

Additive white Gaussian noise with a signal-to-noise ratio (SNR) of 20 dB is added to the image pixel measurements, and noise with zero mean and a variance of 0.01 is added to the velocity measurements. The velocity signal is differentiated using the “Derivative” block in Simulink to obtain a linear acceleration signal. The estimates are integrated with a step size of 0.01 s using the “ode4” Matlab command which uses a Runge–Kutta (R-K) integrator. The initial condition of the observer is set to $\alpha(t_0) = 5$ with $k_3 = 1.55 \times 10^{-3}$. For the observer in [27], the initial condition is chosen to be $\zeta(t_0) = -0.9$ and the observer gain is set to 2.5×10^{-5} . The initial conditions and the observer gains for the observer in [26] are selected⁵ as $k_1 = k_2 = 200$, $k_3 = 0.1$ and $\hat{y}_1(t_0) = 600$, $\hat{y}_2(t_0) = 300$, $\hat{y}_3(t_0) = 50$. The initial conditions are selected so that the initial value of the estimated depth is equal for all three observers. A comparison of the depth estimation performance of the observers is shown in Fig. 2. As shown in Table 2, the root-mean square (RMS) of the depth estimation error is also compared for the transient and the steady-state response. The transient period is selected to be the first 0.2 s. The observer presented in this paper has the least transient RMS error, and the observer in [26] has the minimum steady-state RMS error.

A second simulation is performed based on Discussion Point 2 of Section 6. The camera velocities for this simulation are selected as

⁴ The symbol $\zeta(t)$ is taken from [27] and denotes an auxiliary state.

⁵ The symbols $k_1, k_2, k_3, \hat{y}_1(t), \hat{y}_2(t)$ are taken from [26]. The observer in [26] is a third order observer and $\hat{y}_1(t), \hat{y}_2(t)$ denotes the estimates of $y_1(t)$ and $y_2(t)$.

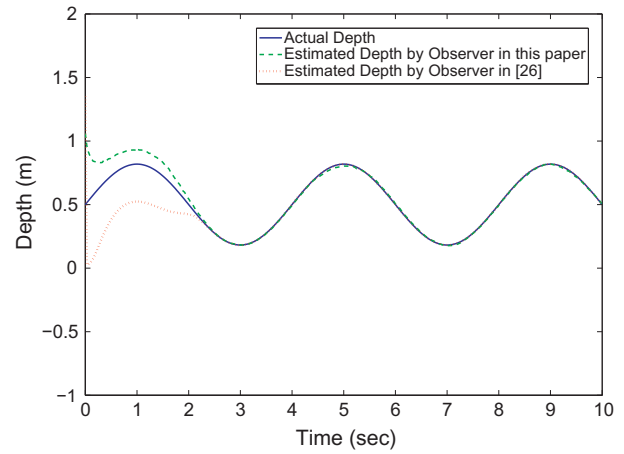


Fig. 3. Comparison of the depth estimation using the observer in this paper and the observer in [26] when camera motion does not satisfy Assumption 2.

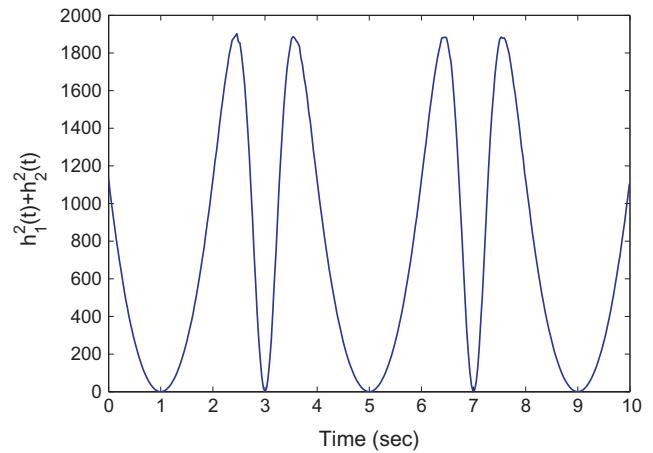


Fig. 4. Evolution of the signal $h_1^2(t) + h_2^2(t)$ against time.

$$b = [0 \ 0 \ 0.5 \ \cos(\pi t/2)]^T \text{ m/s,}$$

$$\omega = [0 \ 0 \ 0]^T \text{ rad/s,}$$

which violates the observability condition in Assumption 2 but satisfies the condition in (26). Again, the image pixel data is corrupted with the additive white Gaussian noise with an SNR of 20 dB. Noise of zero mean and 0.01 variance is added to the camera velocity measurements. Using the Runge–Kutta integrator with a time step of 0.03 s, the state estimates are computed. Fig. 3 shows the depth estimation performance of the observer presented in this paper and the observer in [26] for the same initial conditions $\hat{y}_3(t_0)$. The observer presented in this paper exhibits a better transient performance compared to the observer in [26]. Fig. 4 shows the evolution of $h_1^2(t) + h_2^2(t)$. At 1 s, $h_1^2(t) + h_2^2(t) = 0.1$ and at 3 s, $h_1^2(t) + h_2^2(t) = 10e - 4$. In Fig. 5, there is a peak in the depth estimate of [27] near $t = 1$ s. The response recovers from the peak at $t = 1$ s but at $t = 3$ s the observer in [27] becomes singular. The results in Fig. 5 coincide with the theoretical prediction discussed in Point 2 of Section 6.

A third simulation is performed using camera velocities of

$$b = \left[0.3 \ 0.4 + 0.1 \sin\left(\frac{\pi t}{4}\right) - 1 \right]^T \text{ m/s,}$$

$$\omega = \left[0 \ \frac{\pi}{3} \ 0 \right]^T \text{ rad/s,}$$

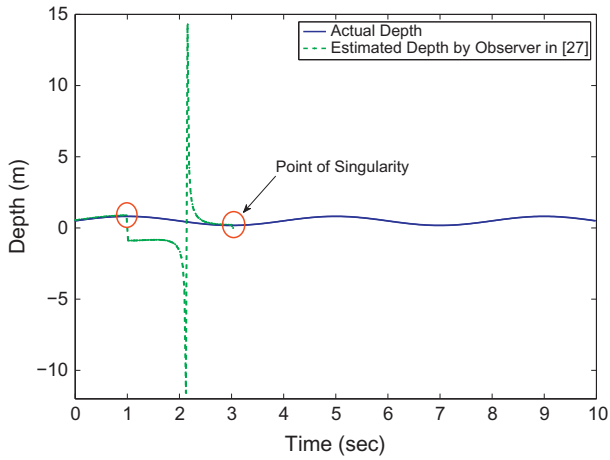


Fig. 5. Depth estimation using the observer in [27].

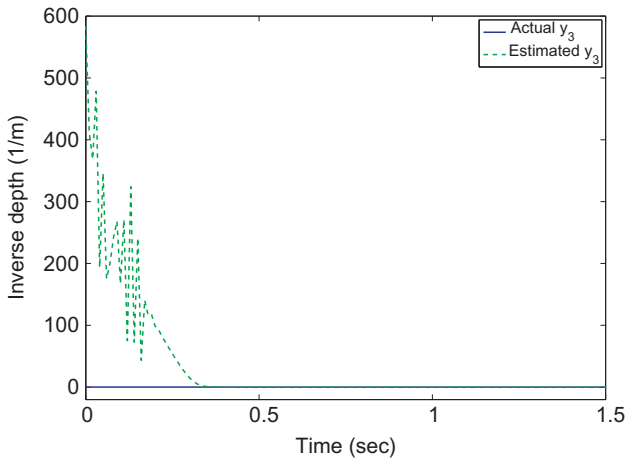


Fig. 6. Estimation of $\hat{y}_3(t)$ starting from large initial condition $\alpha(t_0) = 300$ using the observer in this paper.

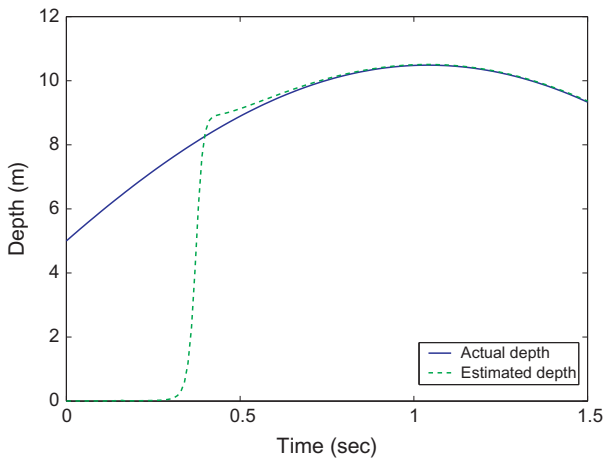


Fig. 7. Depth estimation with large initial condition $\alpha(t_0) = 300$ using the observer in this paper.

to demonstrate that for large initial conditions the observer presented in this paper converges while the local observer in [26] is unstable. In [26], the domain of initial conditions is small for large $b_3(t)$, $\omega_1(t)$ and $\omega_2(t)$. The initial relative position of the target point

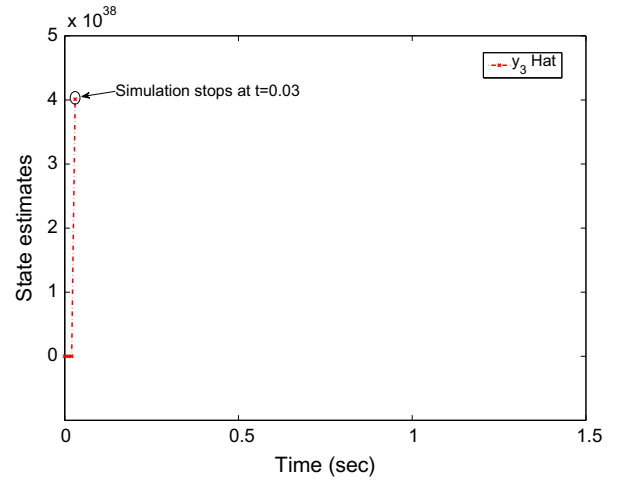


Fig. 8. State estimation using the observer in [26] for large initial conditions. Since the state estimate is very large, simulation fails to integrate at $t = 0.03$.

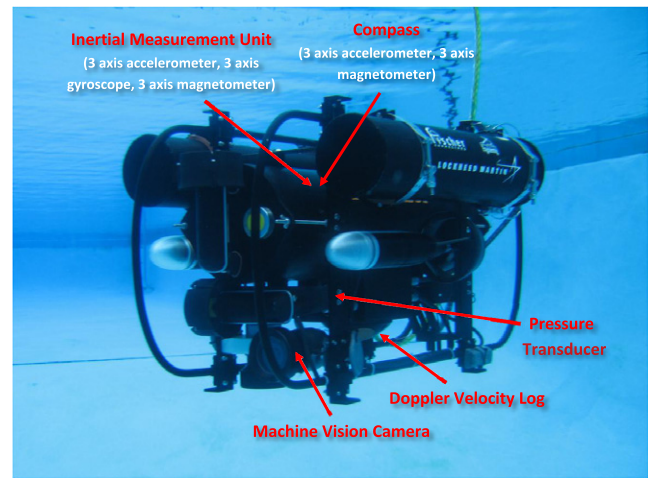


Fig. 9. AUV experimental setup.

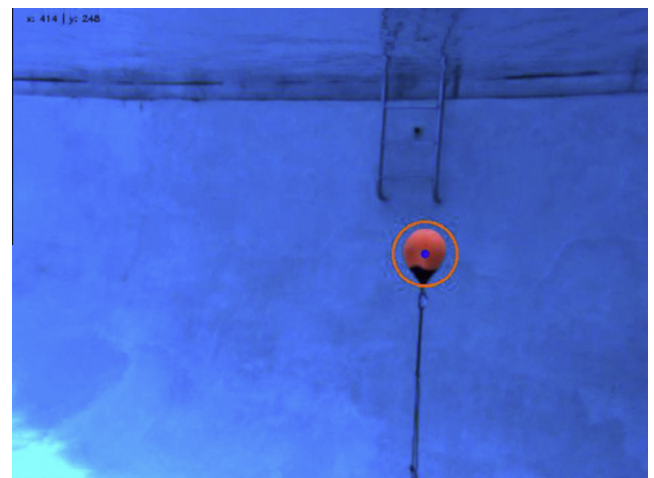


Fig. 10. An ith camera frame displaying the image-based tracking of buoy target.

is $\bar{m}(t_0) = [10 \ 5 \ 5]^T$ m. The observer in this paper is initialized to $\alpha(t_0) = 300$ and the gain is selected as $k_3 = 0.09$. For the observer in [26], the initial conditions and gains are set to

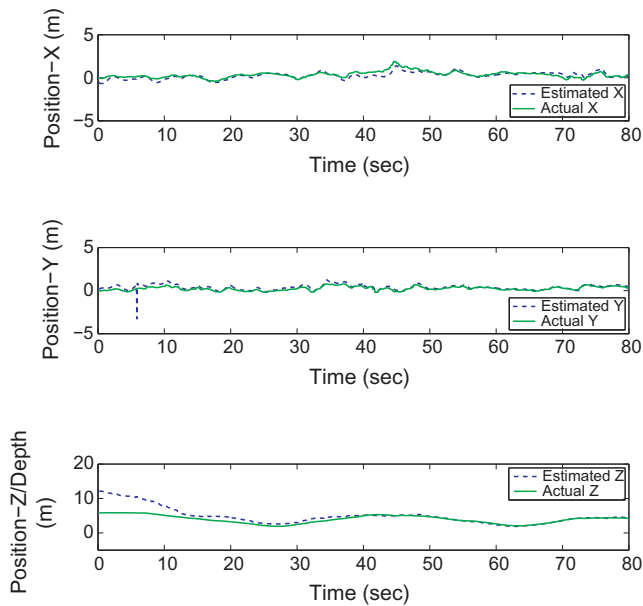


Fig. 11. Comparison of the estimated and ground truth range of the buoy with respect to the underwater vehicle.

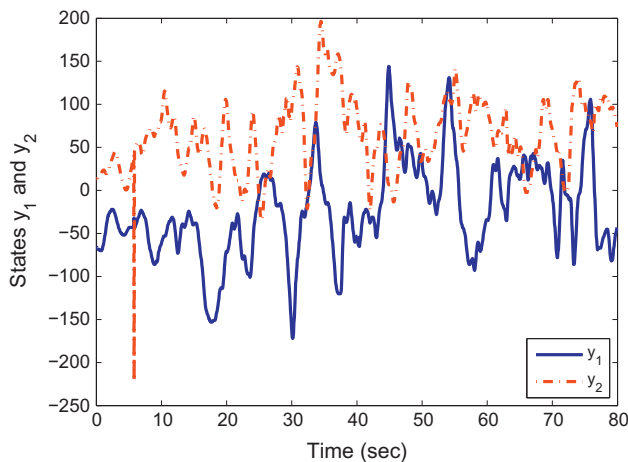


Fig. 12. States $y_1(t)$ and $y_2(t)$ computed using image pixels.

$\hat{y}_1(t_0) = 60$, $\hat{y}_2(t_0) = 30$, $\hat{y}_3(t_0) = 144$ and $k_1 = k_2 = 12$, $k_3 = 10.2$. The observers are integrated using the Runge–Kutta integrator with a time step of 0.01 s. The state estimation results are shown in Figs. 6–8. Since the states $y_1(t)$ and $y_2(t)$ are measurable, the initial conditions of $\hat{y}_1(t)$ and $\hat{y}_2(t)$ are set equal to the initial values of $y_1(t)$ and $y_2(t)$. The gains of the observer in [26] are tuned and the initial condition is progressively increased until the observer error converges. Convergence is observed for $\hat{y}_3(t_0) \leq 143$ but not for $\hat{y}_3(t_0) \geq 144$. For the observer presented in this paper, the observer error converges even for an initial condition as large as $\alpha(t_0) = 300$. In this simulation a value of $\alpha(t_0) = 300$ corresponds to $\hat{y}_3(t_0) = 583.5$ for the proposed observer. The simulation demonstrates that the observer in [26] is unstable when the initial conditions are chosen outside a local domain.

Experiments are conducted to estimate the range of a 9-in. Mooring buoy floating in the middle of a water column as observed by a camera rigidly attached to an autonomous underwater vehicle (AUV). Fig. 9 shows the AUV experimental platform. The AUV is equipped with a Matrix Vision mvBlueFox-120a color USB camera,

a doppler velocity log (DVL), a pressure transducer, a compass and an inertial measurement unit (IMU). Two computers running Microsoft Windows Server 2008 are used on the AUV. One computer is dedicated for running image processing algorithms and the other computer executes sensor data fusion, low level component communication and control, and mission planning. An unscented Kalman filter (UKF) is used to fuse the IMU, DVL and pressure transducer data at 100 Hz to accurately estimate the position, orientation and velocity of the AUV with respect to an inertial frame by correcting the IMU bias. This position data is used to compare the results of the observer with a relative ground truth measurement of the AUV by rotating the localized AUV position into the camera fixed frame. The buoy is tracked in the video image of dimension 640×480 using a standard feature tracking algorithm as shown in Fig. 10, and pixel data of the centroid of the buoy is recorded at 15 Hz. The camera is calibrated using a standard camera calibration algorithm [41] and is given by

$$A = \begin{bmatrix} 749.82231 & 0 & 321.05569 \\ 0 & 750.19507 & 292.41939 \\ 0 & 0 & 1 \end{bmatrix}$$

The linear and angular velocity, and linear acceleration data obtained from the UKF is logged at the camera frame rate. Using the velocity, linear acceleration and pixel data obtained from the AUV sensors, the range of the buoy is estimated with respect to the camera. The initial condition is chosen as $\alpha(t_0) = 0.08$ and the observer gain is selected to be $k_3 = 2 \times 10e-6$. The observer equations are integrated using a Runge–Kutta integrator with a time step of $\frac{1}{15}$ s. A comparison of the estimated range with the ground truth measurement is shown in Fig. 11. In Fig. 12, the feature tracking algorithm fails for several frames near time $t = 6$ s. The range estimation algorithm shows robust performance even in the presence of feature tracking errors as illustrated in Fig. 11.

8. Conclusion

A nonlinear observer is presented for the range estimation of feature points using a moving camera which is globally exponentially stable provided an observability condition is satisfied. The exponential stability of the estimation error is also shown under a relaxed observability condition. The robustness of the observer is characterized using the $\mathcal{L}_2[0, \infty)$ gain from the external disturbance acting on the camera motion and pixel noise to the estimation error. Comparison of the simulation results with the existing observers shows that the proposed observer can be implemented for more general camera motions and larger set of initial conditions. Experimental results demonstrate the robust performance of the observer in the presence of sensor noise.

Acknowledgment

This research is supported in part by the Department of Energy, Grant Number DE-FG04-86NE37967, as part of the DOE University Research Program in Robotics (URPR).

References

- [1] Hartley R, Zisserman A. Multiple view geometry in computer vision. Cambridge University Press; 2003.
- [2] Oliensis J. Exact two-image structure from motion. IEEE Trans Pattern Anal Mach Intell 2002;24(12):1618–2002.
- [3] Oliensis J. A critique of structure-from-motion algorithms. Comput Vis Image Understand 2000;80:172–214.
- [4] Sturm P, Triggs B. A factorization based algorithm for multi-image projective structure and motion. Lect Notes Comput Sci 1996;1065:709–20.
- [5] Bartoli A, Sturm P. Constrained structure and motion from multiple uncalibrated views of a piecewise planar scene. Int J Comput Vision 2003;52(1):45–64.

- [6] Bartoli A, Sturm P. Structure-from-motion using lines: representation, triangulation, and bundle adjustment. *Comput Vis Image Understand* 2005;100(3):416–41.
- [7] Soatto S, Frezza R, Perona P. Motion estimation via dynamic vision. *IEEE Trans Autom Control* 1996;41(3):393–413.
- [8] Hu G, Aiken D, Gupta S, Dixon WE. Lyapunov-based range identification for paracatadioptric systems. *IEEE Trans Autom Control* 2008;53(7):1775–81. doi:10.1109/TAC.2008.928312.
- [9] Chitrakaran V, Dawson DM, Dixon WE, Chen J. Identification of a moving object's velocity with a fixed camera. *Automatica* 2005;41(3):553–62.
- [10] Soatto S, Perona P. Reducing "structure from motion": a general framework for dynamic vision. Part 1: Modeling. *IEEE Trans Pattern Anal Mach Intell* 1998;20(9):933–42.
- [11] Azarbayejani A, Pentland AP. Recursive estimation of motion, structure, and focal length. *IEEE Trans Pattern Anal Mach Intell* 1995;17(6):562–75. doi:http://doi.ieeecomputersociety.org/10.1109/34.387503.
- [12] Chen X, Kano H. State observer for a class of nonlinear systems and its application to machine vision. *IEEE Trans Autom Control* 2004;49(11):2085–91.
- [13] Dixon WE, Fang Y, Dawson DM, Flynn TJ. Range identification for perspective vision systems. *IEEE Trans Autom Control* 2003;48(12):2232–8. doi:10.1109/TAC.2003.820151.
- [14] Quian G, Chellappa R. Structure from motion using sequential Monte Carlo methods. *Int J Comput Vision* 2004;59:5–31.
- [15] Dahl O, Nyberg F, Heyden A. Nonlinear and adaptive observers for perspective dynamic systems. In: *Proc Am control conf, New York City, USA; 2007*. p. 966–71.
- [16] De Luca A, Oriolo G, Giordano P. On-line estimation of feature depth for image-based visual servoing schemes. In: *Proc IEEE int conf robot autom; 2007*. p. 2823–8.
- [17] Jankovic M, Ghosh B. Visually guided ranging from observations points, lines and curves via an identifier based nonlinear observer. *Syst Contr Lett* 1995;25(1):63–73.
- [18] Matthies L, Kanade T, Szeliski R. Kalman filter-based algorithm for estimating depth from image sequence. *Int J Comput. Vision* 1989;3:209–36.
- [19] Kano H, Ghosh BK, Kanai H. Single camera based motion and shape estimation using extended Kalman filtering. *Math Comput Modell* 2001;34:511–25.
- [20] Chiuso A, Favaro P, Jin H, Soatto S. Structure from motion causally integrated over time. *IEEE Trans Pattern Anal Mach Intell* 2002;24(4):523–35.
- [21] Reif K, Unbehauen R. The extended Kalman filter as an exponential observer for nonlinear systems. *IEEE Trans Signal Process* 1999;47(8):2324–8.
- [22] Boutayeb M, Rafaralahy H, Darouach M. Convergence analysis of the extended Kalman filter used as an observer for nonlinear deterministic discrete-time systems. *IEEE Trans Autom Control* 1997;42(4):581–6.
- [23] Reif K, Sonnermann F, Unbehauen R. An EKF-based nonlinear observer with a prescribed degree of stability. *Automatica* 1998;34:1119–23.
- [24] Karagiannis D, Astolfi A. A new solution to the problem of range identification in perspective vision systems. *IEEE Trans Autom Control* 2005;50(12):2074–7. doi:10.1109/TAC.2005.860269.
- [25] Ma L, Cao C, Hovakimyan N, Dixon WE, Woolsey C. Range identification in the presence of unknown motion parameters for perspective vision systems. In: *Proc Am control conf, New York City, USA; 2007*. p. 972–7.
- [26] Luca AD, Oriolo G, Giordano PR. Feature depth observation for image-based visual servoing: theory and experiments. *Int J Robot Res* 2008;27(10):1093–116.
- [27] Morbidi F, Praticchizzo D. Range estimation from a moving camera: an immersion and invariance approach. In: *Proc IEEE int conf robot autom, kobe, Japan, 2009*, pp. 2810–5.
- [28] Lucas B, Kanade T. An iterative image registration technique with an application to stereo vision. In: *Int joint conf artif intell, vol. 3, Citeseer; 1981*. p. 3.
- [29] Lowe DG. Distinctive image feature from scale-invariant keypoints. *Int J Comput Vision* 2004;60:91–110.
- [30] Bay H, Tuytelaars T, Van Gool L. Surf: speeded up robust features. *Lect Notes Comput Sci* 2006;3951:404–17.
- [31] Ma Y, Soatto S, Kosecká J, Sastry S. *An invitation to 3-D vision*. Springer; 2004.
- [32] Hutchinson S, Hager G, Corke P. A tutorial on visual servo control. *IEEE Trans Robot Autom* 1996;12(5):651–70.
- [33] Khalil H. Adaptive output feedback control of nonlinear systems represented by input–output models. *IEEE Trans Autom Control* 1996;41(2):177.
- [34] Chen X, Kano H. A new state observer for perspective systems. *IEEE Trans Autom Control* 2002;47(4):658–63. doi:10.1109/9.995045.
- [35] Chicone C. *Ordinary differential equations with applications*. 2nd ed. Springer; 2006.
- [36] Sastry S, Bodson M. *Adaptive control: stability, convergence, and robustness*. Upper Saddle River (NJ): Prentice Hall; 1989.
- [37] Khalil HK. *Nonlinear systems*. 3rd ed. Prentice Hall; 2002.
- [38] Stefanovic N, Ding M, Pavel L. An application of L2 nonlinear control and gain scheduling to erbium doped fiber amplifiers. *Control Eng Pract* 2007;15:1107–17.
- [39] Kelly R, Santibanez V, Loria A. *Control of robot manipulators in joint space*. Springer; 2005.
- [40] Nagata F, Kuribayashi K, Kiguchi K, Watanabe K. Simulation of fine gain tuning using genetic algorithms for model-based robotic servo controllers. In: *Proc int sym comput intell robot autom; 2007*. p. 196–201.
- [41] Zhang Z. A flexible new technique for camera calibration. *IEEE Trans Pattern Anal Mach Intell* 2000;22(11):1330–4.